Journal of the Taiwan Institute of Chemical Engineers 90 (2018) 9–17

Contents lists available at ScienceDirect

Journal of the Taiwan Institute of Chemical Engineers

journal homepage: www.elsevier.com/locate/jtice

Numerical investigation on the influence of air flow in a die filling process

Huaqin Yao[a,*], Yuki Mori[a], Kazuya Takabatake[a], Xiaosong Sun[b], Mikio Sakai[b,*]

[a] Department of Nuclear Engineering and Management, School of Engineering, The University of Tokyo, 7-3-1 Hongo, Bunkyo-ku, Tokyo 113-8656, Japan
[b] Resilience Engineering Research Center, School of Engineering, The University of Tokyo, 7-3-1 Hongo, Bunkyo-ku, Tokyo 113-8656, Japan

ARTICLE INFO

Article history:
Received 10 July 2017
Revised 23 October 2017
Accepted 27 November 2017
Available online 26 December 2017

Keywords:
DEM-CFD method
Signed distance function
Immersed boundary method
Die filling

ABSTRACT

Die filling is an important manufacturing process that is widely involved in material science and technology in chemical engineering. Application of numerical technologies is desired in optimizing a die filling process. The Discrete Element Method (DEM) is widely used to simulate granular flows in die filling. However, the existing DEM has a problem regarding the computation of air flow in a moving shoe system, even though the DEM is coupled with computational fluid dynamics (CFD). This is because that the simulation of a gas-solid flow with a moving boundary requires an extremely complex algorithm. In order to solve this problem, The Advanced DEM-CFD method is proposed to calculate granular particles interacting with air meanwhile during the whole die filling process. In the Advanced DEM-CFD method, a compact algorithm is employed to simulate a gas-solid flow in a moving boundary system, where wall boundary is modeled by Signed Distance Function and Immersed Boundary Method for solid phase and fluid phase. Validation tests are performed to show the adequacy of the Advanced DEM-CFD method. The results show that the simulations well agree with the experiments, and hence our numerical approach is adequate to reproduce actual die filling processes.

1. Introduction

Die filling is an important manufacturing process in material science and technology in chemical engineering. The fundamental components of a die filling system includes a die, a shoe and a table, along which the shoe containing millions of fine particles can move to the deposition area and formulate particles under the gravity [1,2]. The formulation of the particles is during the filling procedure and they are shaped into a rigid pile inside the die, during which the particles interacting with air and arbitrary geometry is happening all the time. Such kind of a gas-solid flow is examined and studied frequently in pharmaceuticals and powder metallurgy [3,4] in order to improve the quality and efficiency among the relative applications by re-evaluating the properties of the particles, devices as well as the products. A growing attention has been paid on these processes to decide the efficiency of a die filling system [5] by evaluating the states of the system at different collapsed time points. Nevertheless, it is extreme time-consuming and economically unviable for sensitivity studies of a die filling system. New geometries are changeful since adjusting to a better condition is based on a huge number of tests and experiments. It is desirable that the optimization of a die filling process is able to be realized by using 3D modeling and numerical method. The development and application of computational modeling becomes important to accomplish the study of the powder behavior during die filling process.

The Discrete Element Method (DEM) [6] is effective for reproducing particle movements. It is governed by the equation of Newton's second law of motion, in which the external forces with particles and wall boundary are physically accounted. Nowadays the DEM is applied in many fields [7], *e.g.*, pneumatic conveying [8], a fluidized bed [9–13], a packed bed [14], a blender [15]. Since the Signed Distance Function (SDF) [16] was developed to present the wall boundaries by setting a scalar field, complex shape vessel could be simulated by the DEM [17–19]. Consequently, the DEM has been applied to various industrial systems.

As far as application of the DEM to the die filling is concerned, the DEM simulations were performed without air flow and under simple systems. In previous study [20], the air flow was simulated in limited area in die-filling as thus the gas-solid flow could not be simulated completely in the whole processes. In recent studies [21,22], complex shape die was employed, where the wall boundary was modeled by meshes. Very recently, complicated die geometries could be created easily by introducing the new

* Corresponding authors.
E-mail addresses: huaqin_yao@dem.t.u-tokyo.ac.jp (H. Yao), mikio_sakai@n.t.u-tokyo.ac.jp (M. Sakai).

https://doi.org/10.1016/j.jtice.2017.11.031
1876-1070/

technology such as SDF into the DEM (DEM/SDF) [23]. Adequacy of the DEM/SDF was proved through validation tests in die-filling. On the other hand, the DEM/SDF could not simulate the air flow, since solid-fluid interaction model was not introduced into in the DEM/SDF model. Very recently, the authors' group developed a new solid-fluid interaction model [24], where the SDF was combined with the Immersed Boundary Method (IBM) [25,26]. In this method, wall boundary conditions of fluid phase could be simulated by the IBM, where local volume fraction was evaluated based upon the SDF. In an actual die filling system, modeling of granular flow involving air flow, moving shoe system and arbitrary shaped die is required. By using existing numerical simulation techniques, those actual conditions could not be simulated in die filling system. A gas-solid flow in die filling is facing the requirement of a more advanced modeling method. In order to solve this problem, the Advanced DEM-CFD method is newly developed, where the combination of the SDF and IBM is introduced into the DEM-CFD method. Adequacy of the Advanced DEM-CFD method is proved through validation tests in this study.

2. Numerical modeling

2.1. Solid phase

The Advanced DEM-CFD method was applied to perform a simulation of a gas-solid flow in die-filling. The solid phase was modeled by the DEM. In the DEM, the motion of every single particle is governed by Newton's second law of motion as,

$$m\frac{d\boldsymbol{v}}{dt} = \sum \boldsymbol{F_C} + \boldsymbol{F_d} - V_s\nabla p + \boldsymbol{F_g} \tag{1}$$

$$I\frac{d\boldsymbol{\omega}}{dt} = \boldsymbol{T} \tag{2}$$

where m, $\boldsymbol{v}$, t, $\boldsymbol{F_C}$, $\boldsymbol{F_d}$, V_s, P, $\boldsymbol{F_g}$, I, $\boldsymbol{\omega}$ and $\boldsymbol{T}$ represent the mass of the particle, translational velocity of the particle, time, contact force, drag force, particle volume, pressure, gravitational force, moment of inertia of the particle, rotational velocity of the particle and torque, respectively. According to the equation, the total force acting on the particles is composed of the contact force between particles, drag force interacting with the fluid, force due to pressure gradient and gravitational force. The contact force can be divided into two directions, normal and tangential as the equation shows,

$$\boldsymbol{F_C} = \boldsymbol{F_{C_n}} + \boldsymbol{F_{C_t}} \tag{3}$$

where subscript n and t represent the normal and the tangential component. Normal component of the contact force is modeled using a spring and a dashpot, and expressed by

$$\boldsymbol{F_{C_n}} = -k\boldsymbol{\delta_n} - \eta\boldsymbol{v_n} \tag{4}$$

where k, η, $\boldsymbol{\delta_n}$ and $\boldsymbol{v_n}$ represent spring constant, damping coefficient, displacement and the relative velocity of solid particles in normal direction. The damping coefficient is acquired based on the energy dissipation,

$$\eta = -2(\ln e)\sqrt{\frac{mk}{\pi^2 + (\ln e)^2}} \tag{5}$$

where e represents the restitution coefficient.

The tangential component of the contact force is given by

$$\boldsymbol{F_{C_t}} = \begin{cases} -k\boldsymbol{\delta_t} - \eta\boldsymbol{v_t} & (|\boldsymbol{F_{C_t}}| \le \mu|\boldsymbol{F_{C_n}}|) \\ -\mu|\boldsymbol{F_{C_n}}|\dfrac{\boldsymbol{v_t}}{|\boldsymbol{v_t}|} & (|\boldsymbol{F_{C_t}}| > \mu|\boldsymbol{F_{C_n}}|) \end{cases} \tag{6}$$

where μ represents friction coefficient.

The drag force acting on a solid particle is given by

$$\boldsymbol{F_d} = \frac{\beta}{1-\varepsilon}\left(\boldsymbol{u_f} - \boldsymbol{v}\right)V_s \tag{7}$$

where ε, $\boldsymbol{u_f}$, and β are the void fraction, the fluid velocity and interphase momentum transfer coefficient respectively. We use Ergun [27] and Wen-Yu [28] equations to acquire the momentum exchange coefficient. The drag force of both dilute and dense gas-solid flow can be precisely computed by the model. A void fraction of 0.8 is adopted as the boundary between these two equations in the evaluation of β. The β is given by:

$$\begin{cases} \beta_{Ergun} = 150\dfrac{(1-\varepsilon)^2}{\varepsilon}\dfrac{\mu_f}{d_s^2} + 1.75(1-\varepsilon)\dfrac{\rho_f}{d_s}\left|\boldsymbol{u_f} - \boldsymbol{v}\right| & (\varepsilon \le 0.8) \\ \beta_{Wen-Yu} = \dfrac{3}{4}C_d\dfrac{\varepsilon(1-\varepsilon)}{d_s}\rho_f\left|\boldsymbol{u_f} - \boldsymbol{v}\right|\varepsilon^{-2.65} & (\varepsilon > 0.8) \end{cases} \tag{8}$$

In Eq. (8), μ_f represents the fluid viscosity, ρ_f represents the fluid density and d_s is the solid particle diameter. C_d corresponding to the drag coefficient is obtained by the following equation,

$$C_d = \begin{cases} \dfrac{24}{Re_s}\left(1 + 0.15{Re_s}^{0.687}\right) & (Re_s \le 1000) \\ 0.44 & (Re_s > 1000) \end{cases} \tag{9}$$

and the dimensionless particle Reynolds number expressed as Re_s is given by the equation,

$$\mathrm{Re}_s = \frac{\left|\boldsymbol{u_f} - \boldsymbol{v}\right|\varepsilon\rho_f d_s}{\mu_f} \tag{10}$$

2.2. Gas phase

The continuum fluid phase, or gas phase, is governed by continuity equation and Navier-Stokes equation, where local volume average technique is applied [29],

$$\frac{\partial\varepsilon}{\partial t} + \nabla\cdot\left(\varepsilon\boldsymbol{u}_f\right) = 0 \tag{11}$$

$$\frac{\partial\left(\varepsilon\rho_f\boldsymbol{u}_f\right)}{\partial t} + \nabla\cdot\left(\varepsilon\rho_f\boldsymbol{u}_f\boldsymbol{u}_f\right) = -\varepsilon\nabla p - \boldsymbol{f} + \nabla\cdot(\varepsilon\boldsymbol{\tau}) + \varepsilon\rho_f\boldsymbol{g} \tag{12}$$

where $\boldsymbol{f}$ and $\boldsymbol{\tau}$ represent the interaction between gas-solid phases and the viscous stress. $\boldsymbol{f}$ is defined according to Newton's third law of motion:

$$\boldsymbol{f} = \frac{\sum_{i=1}^{N_{grid}}\boldsymbol{F_d}}{V_{grid}} \tag{13}$$

where N_{grid} is the number of solid particles located in the local grid and V_{grid} is the cell volume. $\boldsymbol{F_d}$ is given by Eq. (7).

2.3. Wall boundary modeling

The wall boundary modeling has always been an important part in numerical simulations. In the Advanced DEM-CFD method, combination of the SDF and the IBM was employed for a moving wall boundary in die-filling. Wall boundary modeling of the Advanced DEM-CFD method is briefly addressed for solid and fluid phase as below.

2.3.1. SDF based wall boundary for solid phase

In this study, SDF was employed for creating the wall boundary. The SDF is denoted as $\phi(\boldsymbol{x})$, which is expressed as:

$$\phi(\boldsymbol{x}) = d(\boldsymbol{x})\cdot s(\boldsymbol{x}) \tag{14}$$

where $d(\boldsymbol{x})$ represents the minimum distance pointing from the surface of the geometry structure and $s(\boldsymbol{x})$ represents the sign of

the position of the point where positive indicates that $\boldsymbol{x}$ is inside the structure and vice versa. The contact force can be expressed as the gradient of the kinetic energy. Mathematically, the normal and tangential components of the contact force are expressed as,

$$\boldsymbol{F}_{C_n}^{SDF} = -k\boldsymbol{\delta}_n^{SDF}|\nabla\phi| - \eta\boldsymbol{v}_n \tag{15}$$

$$\boldsymbol{F}_{C_t} = \begin{cases} -k\boldsymbol{\delta}_t^{SDF} - \eta\boldsymbol{v}_t & (|\boldsymbol{F}_{C_t}| \le \mu|\boldsymbol{F}_{C_n}|) \\ -\mu|\boldsymbol{F}_{C_n}|\dfrac{\boldsymbol{v}_t}{|\boldsymbol{v}_t|} & (|\boldsymbol{F}_{C_t}| > \mu|\boldsymbol{F}_{C_n}|) \end{cases} \tag{16}$$

where the superscript SDF indicate the overlap between particle and SDF based wall. The detail description can be found in literature [16].

2.3.2. IBM based wall boundary for gas phase

The IBM is able to simulate solid-fluid interaction based on local volume fraction. In the IBM, velocity field is calculated based on volume average of the local fluid velocity and the local solid object velocity in each calculation grid. The solid-fluid interaction is evaluated based on the local volume fraction of a solid object, where the body force is proportional to the local volume fraction of the solid object. The grid size must be sufficiently smaller than the solid object. In the Advanced DEM-CFD method, the local volume of the solid object is calculated based on the SDF. Combination of the SDF and IBM makes it possible to evaluate the solid-fluid interaction of a moving object easily and accurately. The solid-fluid interface velocity is considered as a projection from solid object onto the fluid and furtherly influences the fluid velocity. Hence, the solid-fluid interaction force given at the interface works to enforce the no-slip condition in the solid-fluid mixture grid.

In the Navier-Stokes equation, instead of calculating the fluid velocity, the velocity field $\boldsymbol{u}$ is established as,

$$\boldsymbol{u} = (1-\alpha)\boldsymbol{u}_f + \alpha\boldsymbol{U}_B \tag{17}$$

where α and $\boldsymbol{U}_B$ represent the local volume fraction obtained by SDF and the boundary velocity.

After substituting the net velocity field for fluid velocity, a correction term $\boldsymbol{f}_{IB}$ must be considered in the original Navier-Stokes equation,

$$\frac{\partial(\varepsilon\rho_f\boldsymbol{u})}{\partial t} + \nabla\cdot(\varepsilon\rho_f\boldsymbol{u}\boldsymbol{u}) = -\varepsilon\nabla p - \boldsymbol{f} + \nabla\cdot(\varepsilon\boldsymbol{\tau}) + \varepsilon\rho_f\boldsymbol{g} + \boldsymbol{f}_{IB} \tag{18}$$

where

$$\boldsymbol{f}_{IB} = \frac{\alpha\rho_f(\boldsymbol{U}_B - \boldsymbol{u}_f)}{\Delta t} \tag{19}$$

The detailed description can be found in literatures [24,25].

3. Validation conditions

3.1. Experimental conditions

NONPAREIL-108® particle (FREUND CORPORATION, Tokyo, Japan) was employed in the current study. Fig. 1 shows the Scanning Electron Microscope (SEM) image of the particle. The diameter of the particle was around 200 μm. The particle density was measured to be 1379 kg/m^3. By using Atomic Force Microscope, the cohesive force acting on the particle was measured and the Hamaker constant was obtained to be 4.4×10^{-22} J.

In the present study, experiments with different initial conditions were performed as listed in Table 1. Dimension of experimental device including two different die position setups is shown in Fig. 2. Each of the setting contains a die, a shoe and a shoe table. The die is a 10 mm's cubic structure with a 5 mm's foursquare

Table 1
Experimental conditions.

Case	Shoe speed	Die position
Case 1-Exp	0.10 m/s	Position 1
Case 2-Exp	0.047 m/s	Position 1
Case 3-Exp	0.10 m/s	Position 2
Case 4-Exp	0.047 m/s	Position 2

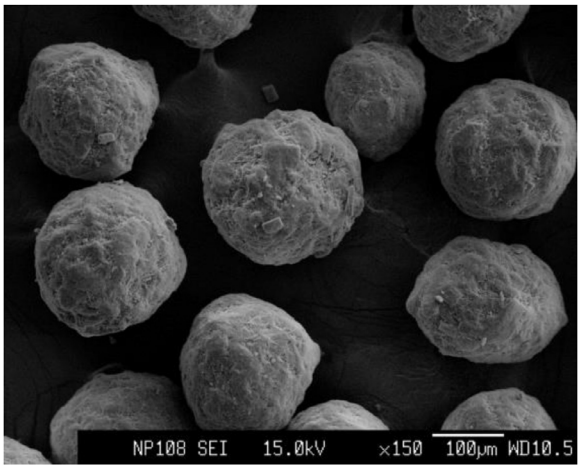

Fig. 1. SEM image of NONPAREIL-108® particle.

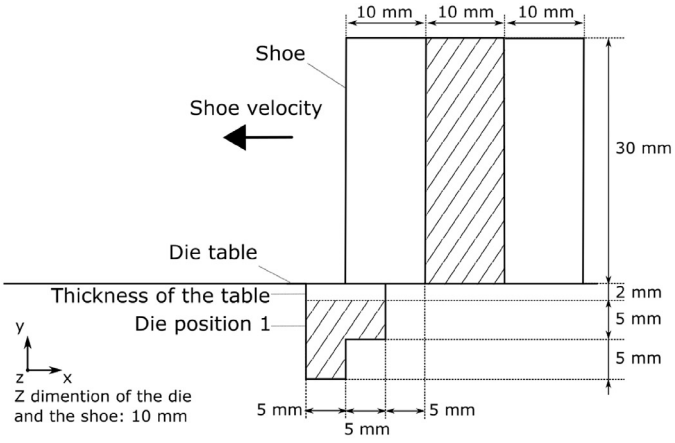

(a) Position 1

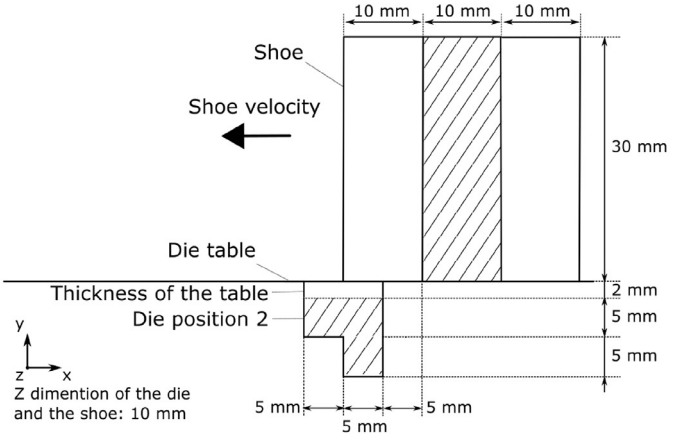

(b) Position 2

Fig. 2. Schematic view of the die filling system.

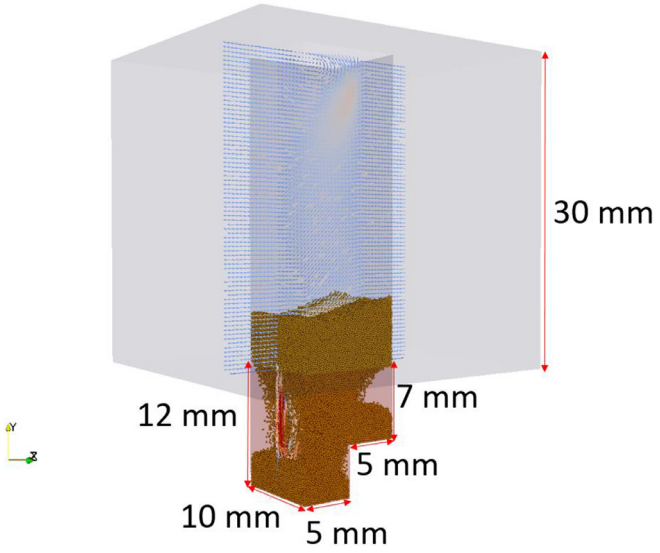

Fig. 3. 3D geometry of the die filling system (Die: Position 1).

hollowed out at bottom corner of the die. The dimension of the shoe cavity is 10 mm × 30 mm × 10 mm in x, y and z directions. A distance of 5 mm between the shoe cavity and the deposition area is set initially. There is a 2 mm thickness considered for the die table. Two kinds of shoe speeds and die positions were tested as different initial conditions. All the experiments were exposed to room air at normal temperature and pressure. Powder injection process was recorded using high speed camera FASTCAM Mini WX 100 (PHOTRON, Tokyo, Japan).

3.2. Calculation conditions

The geometrical diagram of the die filling system with die position 1 is shown in Fig. 3. The geometry was created faithfully based on the experimental device. A cross-sectional slice of the fluid velocity field is expressed to show that how the air flow behave under a moving boundary system. Table 2 shows the calculation conditions. In this study, solid flows and gas-solid flows were both calculated in order to investigate the effect of air flow on particle behavior. The DEM/SDF and the Advanced DEM-CFD method applied for solid flows and gas-solid flows are referred to as “Sim-S” and

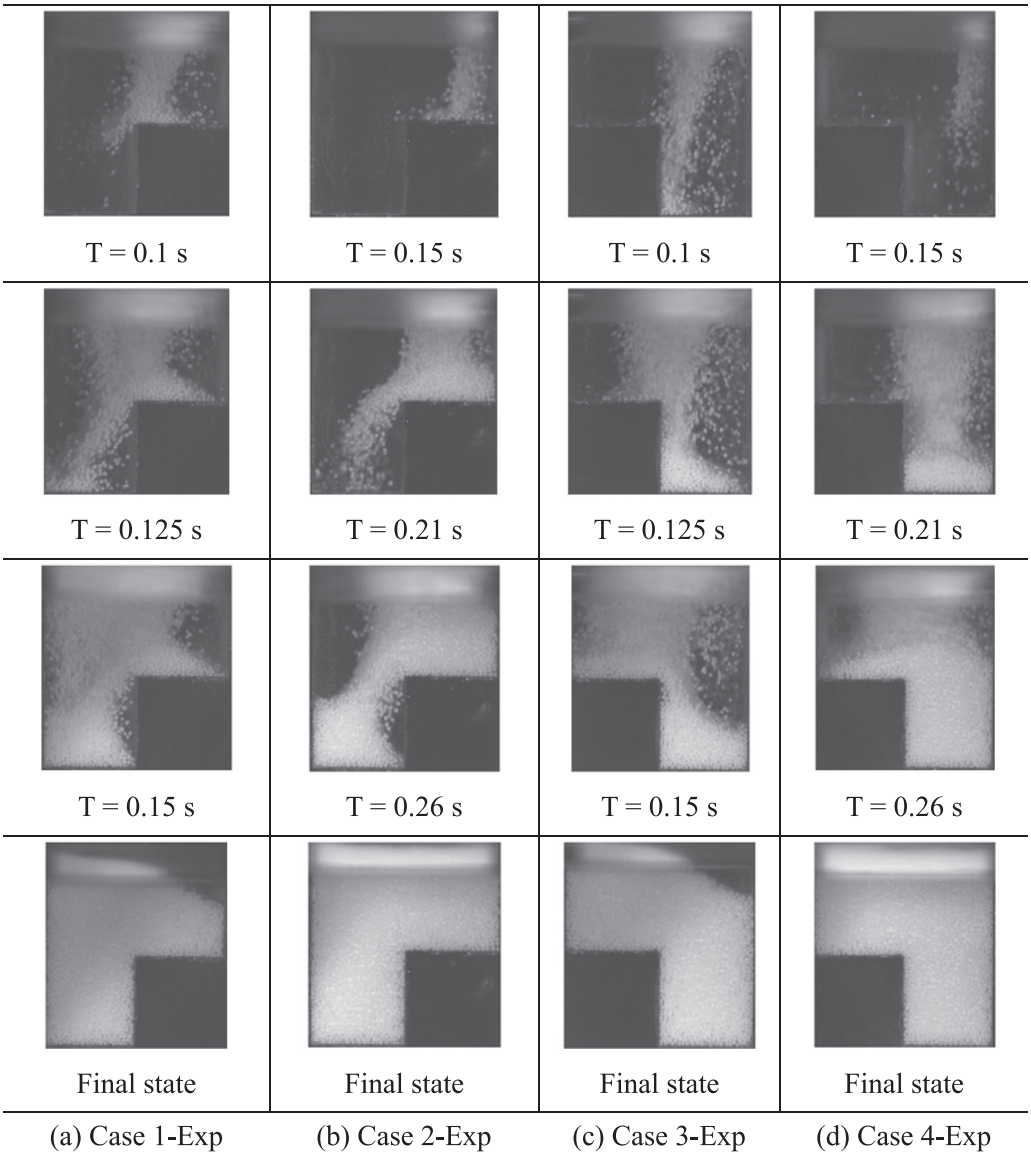

Fig. 4. Experimental results.

Table 2
Calculation conditions.

Case	Phase	Shoe speed	Die position
Case 1-Sim-S	Solid	0.10 m/s	Position 1
Case 1-Sim-GS	Gas & Solid	0.10 m/s	Position 1
Case 2-Sim-S	Solid	0.047 m/s	Position 1
Case 2-Sim-GS	Gas & Solid	0.047 m/s	Position 1
Case 3-Sim-S	Solid	0.10 m/s	Position 2
Case 3-Sim-GS	Gas & Solid	0.10 m/s	Position 2
Case 4-Sim-S	Solid	0.047 m/s	Position 2
Case 4-Sim-GS	Gas & Solid	0.047 m/s	Position 2

Table 3
Physical properties.

Solid phase		
Particle number	–	150,000
Particle diameter	μm	200
Particle density	kg/m^3	1379
Spring constant	N/m	50
Coefficient of restitution	–	0.9
Coefficient of friction	–	0.3
Hamaker constant	J	44×10^{-22}
Gas phase		
Air density	kg/m^3	1.0
Air viscosity	Pa·s	1.8×10^{-5}

"Sim-GS" respectively in Table 2. Each group had the same initial condition corresponding to the experiment test. Two kinds of shoe speeds and die positions were considered in these calculations.

The physical properties of the particle and air are shown in Table 3. 150,000 particles were generated for the test whose initial conditions were obtained by random packing. Particle size, particle density and Hamaker constant were assumed to be respectively 200 μm, 1379 kg/m^3 and 4.4×10^{-22} J corresponding to NONPAREIL-108® particle. The cohesive force due to Van der Waals force is sufficiently smaller than gravitational force. In this study, there is hardly any particle agglomeration occurred and hence we decided to use Ergun and Wen-Yu's equation. Spring constant, restitution coefficient and frictional coefficient were 50 N/m, 0.9 and 0.3, respectively.

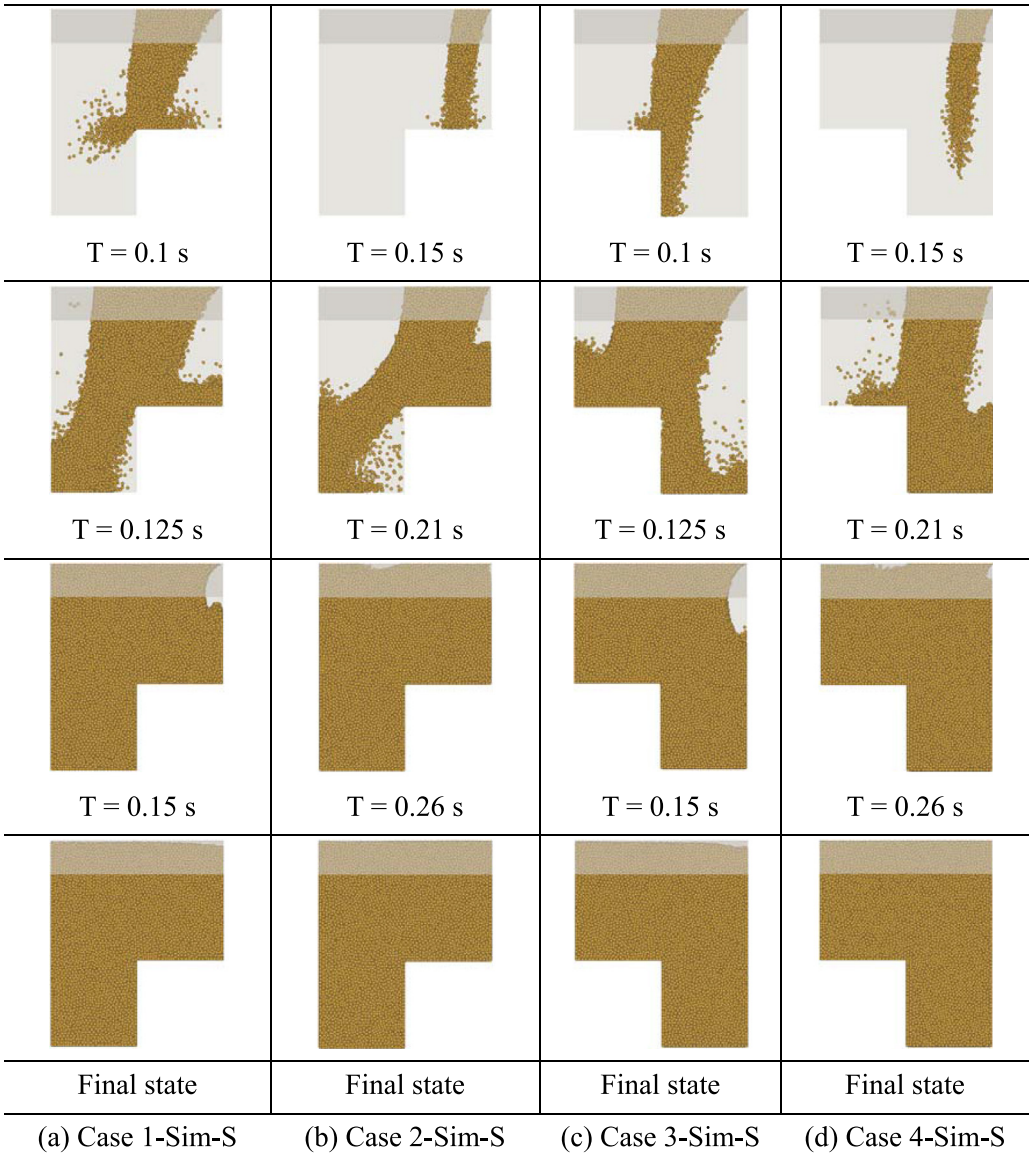

Fig. 5. Particle spatial distribution obtained from the DEM/SDF.

4. Results and discussion

4.1. Experiment

Fig. 4 illustrates the snapshots obtained from experiments. In the experiment for 0.10 m/s shoe speed, namely Case 1-Exp and 3-Exp, snapshots was obtained in 0.1 s, 0.125 s, 0.15 s and final state. In 0.047 m/s of shoe speed, namely Case 2-Exp and 4-Exp, snapshots was obtained in 0.15 s, 0.21 s, 0.26 s and final state. In order to investigate effect of the shoe speed on powder injection in die position 1, we compared the results between Case 1-Exp and 2-Exp. The powder falling velocity was influenced by a shoe velocity. Besides, when the shoe speed was relatively-slow, the filling rate became high. Especially, when the shoe speed was 0.10 m/s (Case 1-Exp), the powder was not fully filled in the die. As far as the reversed direction of the die was concerned, tendency of the filling rate in position 2 was the same as that of the position 1. When the shoe speed was relatively-high such as Case 3-Exp, the powder was not fully filled unlike Case 4-Exp. Consequently, the powder filling rate was shown to be influenced by shoe speed.

4.2. Numerical simulation for single particle phase

Fig. 5 designates the snapshots in the numerical simulations using the DEM/SDF (single solid phase). Elapsed time of the snapshots corresponded to that of the experiments. In order to examine effect of the shoe speed on powder injection in position 1, Cases 1-Sim-S and 2-Sim-S were compared. The filling efficiency of calculations was much higher than that of experiments. The powder filling rate became almost full, even the shoe speed was relatively-high, namely, Case 1-Sim-S. There were differences of powder filling efficiency and filling rate between the simulation and the experiment. We believe that not considering drag force is the main reason for those differences. Hence, modeling of the drag force acting on a particle might be shown to be important in this die filling system.

4.3. Numerical simulation for gas-particle flow

Fig. 6 shows the snapshots of the computation results using the Advance DEM-CFD method. Elapsed time of the snapshots corresponded to that of the experiments. By the same manner as previous sections, Cases 1-Sim-GS and 2-Sim-GS were compared to examine influence of the shoe speed on powder injection in position 2. The filling efficiency of calculations was well agreed with that of experiments. The powder filling rate did not become full when the shoe speed was 0.10 m/s, namely, Case 1-Sim-GS. When the shoe speed was 0.047 m/s, the filling rate was full. In Cases 1 and 2, the filling rate was in good agreement between the

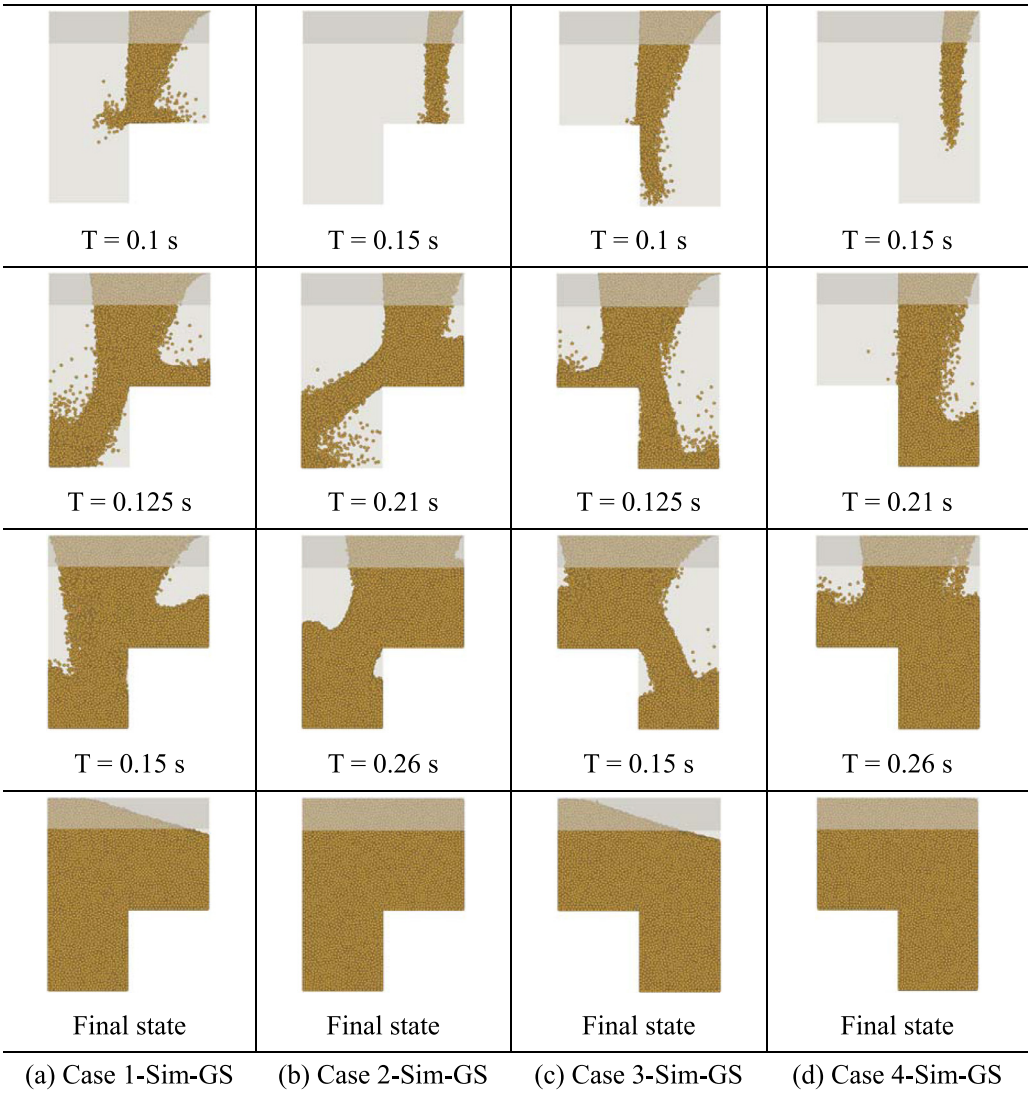

Fig. 6. Particle spatial distribution obtained from the Advanced DEM-CFD method.

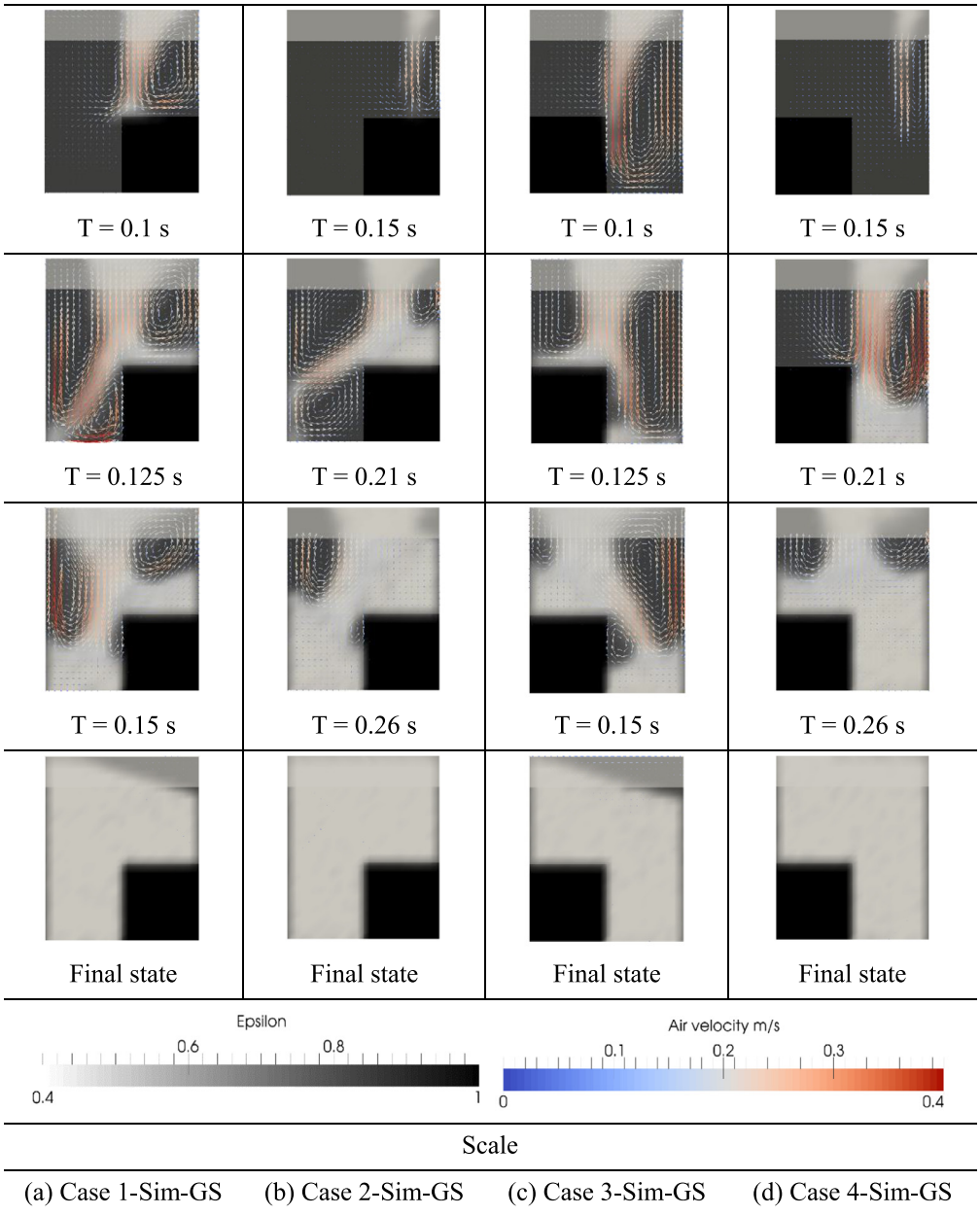

Fig. 7. Volume fraction of solid phase and air flow vector obtained from the Advanced DEM-CFD method.

computations (Sim-GS in Fig. 6(a) & (b)) and experiments (Exp in Fig. 4(a) & (b)). In Cases 3 and 4, powder filling efficiency and filling rate well agreed between the simulation (Fig. 6(c) & (d)) and the experiment (Fig. 4(c) & (d)). This is because not only drag force acting on a solid particle but also gas flow in shoe-die system were modeled suitably. Another figure of the snapshots in gas-solid simulation is illustrated in Fig. 7, where the volume fraction of solid phase as well as the air flow vector inside the die are expressed. With these expressions, the speeds and directions of the air velocity are easy to observe. During the filling process, the highest speed occurred either along with the falling particle flow or near the wall of the die. The air fluid firstly followed the particles going downwards in early stage. Once hitting at the wall or the particle bed, it refluxed backwards and behaved as a counterflow to the particles, during which the injection of the particle was resisted and finally resulted in a less amount of accumulated particles. The quantitative comparison was provided by measuring the distance from the edge of the particle bed to the origin point, which had a fixed level at the right inner surface of the die with an elevation height of 0.7 mm. Fig. 8 shows the edge point distance comparison between the experiment and Sim-GS results in each case. The results from Sim-GS well agreed with the experiment as shown in the graphs. These results indicate that solid-fluid interaction was simulated accurately. Consequently, the modeling of drag force acting on a particle was shown to be adequate through the snapshot comparison between simulations and experiments as well as the quantitative comparison figures.

Conclusions

Numerical simulation of a gas-solid flow in die-filling has hardly been performed so far. This is because that there is a lack of model that is able to simulate a gas-solid flow in moving boundary system by a simple algorithm. In this study, the Advanced DEM-CFD method was developed to simulate a particle flow involving air flow in die filling. In the Advanced DEM-CFD method, combina-

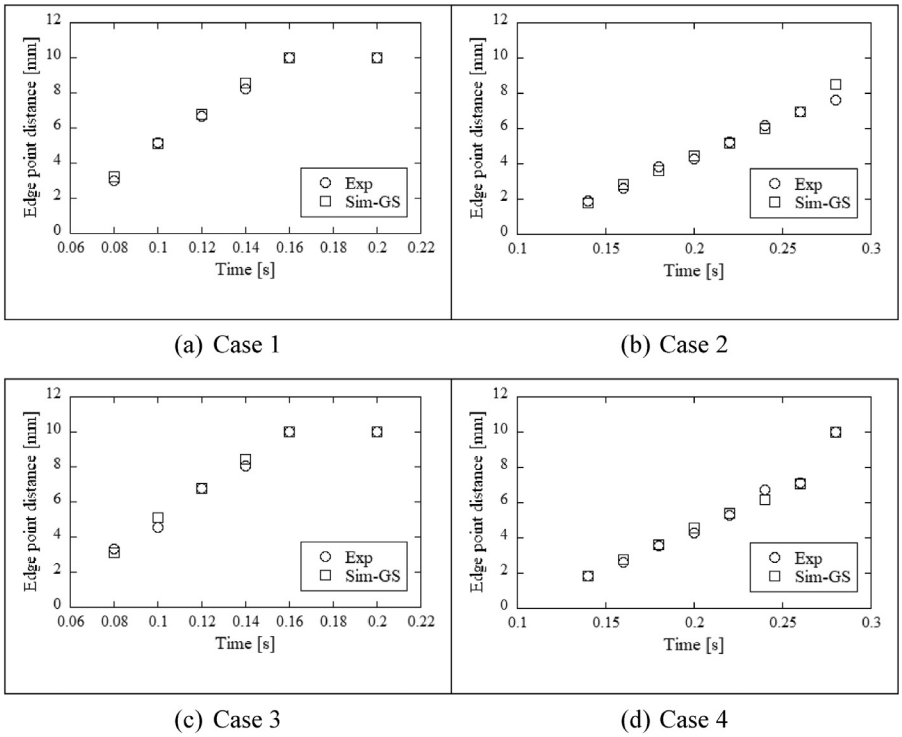

Fig. 8. Edge point distance comparison between experiment and the Advanced DEM-CFD method in 4 cases.

tion of the SDF and IBM was employed for wall boundary model. The combination of the SDF and IBM makes it possible to simulate air flow in a moving boundary such as a shoe easily.

In order to show adequacy of the Advanced DEM-CFD method, 4 types of validation tests were performed. The simulation results well agreed with experimental ones when the gas flow was computed. Especially, the effect of shoe speed on powder filling rate could be accurately simulated by the Advanced DEM-CFD method. Hence, the applicability of the Advanced DEM-CFD method was illustrated through this study. Besides, the injected particle behavior was different in numerical simulations with/without calculating the gas flow. This result implies that the gas flow distinctly influences the solid particle movement in this die-filling system.

Consequently, the Advanced DEM-CFD method was proved to simulate whole particle injection process in die-filling for the first time. This approach has made substantial progress in material technology in chemical engineering.

Acknowledgments

This study was financially supported by JSPS KAKENHI Grant Number: 17H02825. NONPAREIL-108R was provided by FREUND CORPORATION. The authors are grateful to Ms. Yoshie Iijima and Ms. Chie Iguchi for their technical support.

References

[1] Jackson S, Sinka IC, Cocks ACF. The effect of suction during die fill on a rotary tablet press. Eur J Pharm Biopharm 2007;65(2):253–6.
[2] Larsson S, Gustafsson G, Oudich A, Jonsén P, Häggblad H-åke. Experimental methodology for study of granular material flow using digital speckle photography. Chem Eng Sci 2016;155:524–36.
[3] Schneider LCR, Sinka IC, Cocks ACF. Characterisation of the flow behaviour of pharmaceutical powders using a model die-shoe filling system. Powder Technol 2007;173(1):59–71.
[4] Wu CY. DEM simulations of die filling during pharmaceutical tabletting. Particuology 2008;6(6):412–18.
[5] Brewin P, Coube O, Gethin DT, Hodgson H, Rolland S. Modelling of powder die compaction. Springer; 2008.
[6] Cundall PA, Strack ODL. A discrete numerical model for granular assemblies. Géotechnique 1979;29(1):47–65.
[7] Sakai M. How should the discrete element method be applied in industrial systems ?: a review †". *KONA Powder Part*. J 2016;33(33):169–78.
[8] Sakai M, Koshizuka S. Large-scale discrete element modeling in pneumatic conveying. Chem Eng Sci 2009;64(3):533–9.
[9] Sakai M, Abe M, Shigeto Y, Mizutani S, Takahashi H, Vire A, et al. Verification and validation of a coarse grain model of the DEM in a bubbling fluidized bed. Chem Eng J 2014;244:33–43.
[10] Sakai M, Yamada Y, Shigeto Y, Shibata K, Kawasaki VM, Koshizuka S. Large-scale discrete element modeling in a fluidized bed. Int J Numer Meth Fluids 2010;64(10–12):1319–35.
[11] Girardi M, Radl S, Sundaresan S. Simulating wet gas – solid fluidized beds using coarse-grid CFD-DEM. Chem Eng Sci 2016;144:224–38.
[12] Gan J, Zhou Z, Yu A. Particle scale study of heat transfer in packed and fluidized beds of ellipsoidal particles. Chem Eng Sci 2016;144:201–15.
[13] Hosseini SH, Fattahi M, Ahmadi G. CFD study of hydrodynamic and heat transfer in a 2D spouted bed: assessment of radial distribution function. J Taiwan Inst Chem Eng 2016;58:107–16.
[14] Mohanty R, Mohanty S, Mishra BK. Study of flow through a packed bed using discrete element method and computational fluid dynamics. J Taiwan Inst Chem Eng 2016;63:71–80.
[15] Chandratilleke GR, Yu AB, Bridgwater J. A DEM study of the mixing of particles induced by a flat blade. Chem Eng Sci 2012;79:54–74.
[16] Shigeto Y, Sakai M. Arbitrary-shaped wall boundary modeling based on signed distance functions for granular flow simulations. Chem Eng J 2013;231:464–76.
[17] Basinskas G, Sakai M. Numerical study of the mixing efficiency of a batch mixer using the discrete element method. Powder Technol 2016;301:815–29.
[18] Basinskas G, Sakai M. Numerical study of the mixing efficiency of a ribbon mixer using the discrete element method. Powder Technol 2016;287:380–94.
[19] Sakai M, Shigeto Y, Basinskas G, Hosokawa A, Fuji M. Discrete element simulation for the evaluation of solid mixing in an industrial blender. Chem Eng J 2015;279:821–39.
[20] Guo Y, Wu C, Kafui KD, Thornton C. 3D DEM / CFD analysis of size-induced segregation during die filling. Powder Technol 2011;206(1–2):177–88.
[21] Mateo-ortiz D, Méndez R. Relationship between residence time distribution and forces applied by paddles on powder attrition during the die filling process. Powder Technol 2015;278:111–17.
[22] Mateo-Ortiz D, Muzzio FJ, Méndez R. Particle size segregation promoted by powder flow in confined space: the die filling process case. Powder Technol 2014;262:215–22.
[23] Tsunazawa Y, Shigeto Y, Tokoro C, Sakai M. Numerical simulation of industrial die filling using the discrete element method. Chem Eng Sci 2015;138:791–809.
[24] Sun X, Sakai M. Numerical simulation of two-phase flows in complex geometries by using the volume-of- fluid /immersed-boundary method. Chem. Eng. Sci. 2016;139:221–40.

[25] Sun X, Sakai M. Immersed boundary method with artificial density in pressure equation for modeling flows confined by wall boundaries. J Chem Eng Japan 2017;50(3):161–9.
[26] Yuki Y, Takeuchi S, Kajishima T. Efficient immersed boundary method for strong interaction problem of arbitrary shape object with the self-induced flow. J Fluid Sci Technol 2007;2(1):1–11.
[27] Ergun S. Fluid flow through packed columns. Chem Eng Progr 1952;48:89–94.
[28] Wen CY, Yu YH. Mechanics of fluidization. Chem Eng Progr Symp Ser 1966;62:100–11.
[29] Anderson TB, Jackson ROY. A fluid mechanical description of fluidized beds. Ind Eng Chem Fundam 1967;6(4):527–39.